A CASE FOR EDUCATION

Radiofrequency ablation data associated with atrioesophageal fistula

David R. Tomlinson, MD,* John Mandrola, MD†

*From the *University Hospitals Plymouth NHS Trust, South West Cardiothoracic Centre, Derriford Hospital, Plymouth, United Kingdom, and †Baptist Health Louisville, Louisville, Kentucky.*

Introduction

We present detailed analyses of auto-annotated radiofrequency (RF) ablation data from a pulmonary vein isolation (PVI) procedure that was performed using widely accepted methods (30 W, ≤6 mm inter–ablation site distance, ablation index guidance) but still ended with a catastrophic complication. We hope that lessons learned in this case will help inform clinical practice guidelines toward greater safety during atrial fibrillation (AF) ablation.

Case report

History of presentation

A 66-year-old man with a 6-year history of paroxysmal AF underwent initially uncomplicated PVI.

Cardiac computed tomography (CT) performed the day before was normal. Using fentanyl and alfentanil analgesia without additional sedatives, a CARTO® (Biosense Webster Inc, Irvine, CA) 3-D left atrial (LA) electroanatomical map was created using CT image integration. Contact force (CF) point-by-point, power-controlled RF ablation at 30 W was delivered using VISITAG™ and ablation index (AI) guidance, achieving pulmonary vein (PV) entrance and exit block.

The patient was discharged the following day, but he experienced ongoing chest pain and dysphagia. Sixteen days postablation he became febrile and experienced near-syncope with transient hemiparesis. Following hospital admission, urgent CT angiography demonstrated the following: *"Impression of a wall-thickened esophagus where it passes behind the lower left pulmonary vein. The vein is narrow, but no significant stenosis. No contrast leakage / fistulation are detected."* Brain CT was normal. The following day and prompted by upper gastrointestinal bleeding with rapid reduction in Glasgow coma scale, CT brain demonstrated bilateral *"recent infarct changes"* and repeat CT angiography reported *"Suspicion of atrial oesophageal fistula. As a last impression of slightly wall-thickened esophagus where it passes the lower left pulmonary veins. Acquired air locus posteriorly in the left atrium and possible air locus located between esophagus and left atrium / left pulmonary vein."* Blood cultures grew streptococci. The patient was transferred to a nearby cardiothoracic center but was deemed unfit for surgery owing to extensive strokes and sepsis. Repeat CT brain and thorax the following day demonstrated *"countless recent infarcts and probably microbleeds in both cerebral and cerebellar hemispheres"* and *"Large thrombus / vegetation containing air in the left atrium. Near total occlusion of the left lower pulmonary vein."* With conservative treatment, the patient died 3 days later, 21 days post-AF ablation.

Auto-annotated RF data

The patient's family was provided with the CARTO procedure ("Backup") file and kindly forwarded this (to DRT) for analysis. Following reloading onto CARTO, auto-annotated RF data were exported as text files using the proprietary function; unfortunately, no electrograms were available for analysis. Data were imported to Excel, with statistical analyses performed using GraphPad Prism; inter–ablation site (ie, tag) distances were obtained online using the distance measurement tool. No details of autopsy findings were available.

Total procedure RF duration was 44 minutes: 20 and 24 minutes for left- and right-sided PVs, respectively. Table 1 shows a comparison of left vs right PV-isolating auto-annotated tags. There was no significant difference comparing left PV vs right PV-isolating tags regarding median RF duration (19.6 seconds vs 18.3 seconds), mean CF (16.8 g vs 15.8 g), and AI (421 vs 404) achieved. However, the impedance drop was significantly greater at left vs right PV-isolating tags (9.7 Ω vs 8.2 Ω, $P = .02$).

Figure 1 shows VISITAG auto-annotation preferences and the final lesion set achieved: tag radius was set to 3

Test your knowledge!
Take an interactive quiz related to this article: https://www.heartrhythmcasereports.com/content/quiz_archive

KEYWORDS Atrioesophageal fistula; Atrial fibrillation; Contact force catheter ablation; Complications; Pulmonary vein isolation; Radiofrequency ablation
(Heart Rhythm Case Reports 2021;7:781–790)

Funding: None. Conflict of interest: The authors have no conflicts to declare. **Address reprint requests and correspondence:** David R. Tomlinson, University Hospitals Plymouth NHS Trust, South West Cardiothoracic Centre, Derriford Hospital, Derriford Rd, Plymouth, PL6 8DH, UK. E-mail address: david.tomlinson1@nhs.net.

https://doi.org/10.1016/j.hrcr.2021.09.012

Table 1 Auto-annotated radiofrequency ablation data

	Left-sided sites	Right-sided sites	*P*
Number of tags	52	63	NA
RF duration (s)	19.6 (8.6–36.4)	18.3 (6.2–30.2)	.66
Mean CF (g)	16.8 (9.7–24.4)	15.8 (9.7–23.0)	.60
Ablation index	421 (323–529)	404 (299–513)	.44
Impedance drop (Ω)	9.7 (6.4–14.9)	8.2 (4.0–10.5)	.02

Exported VISITAG data according to left- vs right-sided pulmonary vein isolating sites; data shown are median (first and third quartiles).
CF = contact force; NA = not applicable; RF = radiofrequency.

mm during the case, indicating target intertag distance ≤6 mm. Figure 2 also displays these same tags but using impedance drop coloration. Notably, a cluster of closely spaced tags can be seen at the posterior wall opposite the left inferior PV in the vicinity of where the atrioesophageal fistula (AEF) was subsequently noted; this site underwent detailed analysis.

Table 2 shows auto-annotated RF data for all 11 tags delivered at the LA posterior wall (LAPW) region associated with AEF. Median (range) RF duration, mean CF, and AI were 18.7 seconds (3.8–38.5 seconds), 22.3 g (15.2–37.7 g), and 406 (285–578), respectively. Notably, median impedance drop was 13.6 Ω – that is, far greater than that achieved for the total left PV-isolating tags. The greatest impedance drop (ie, 42.2 Ω) occurred during the first RF application in this region (tag 24), following just 10.5 seconds RF with mean CF 20.6 g, and AI 354 (Figure 2). Moreover, the first 3 annotated tags in this region totaled 51 seconds, achieving the greatest impedance drops in the entire case of 42.2 Ω, 23.3 Ω, and 27.2 Ω, and with AI 354, 535, and 418, respectively.

As an indication of possible "thermal stacking"—that is, excessive deep thermal effects owing to close spatial and temporal relationships between consecutive RF applications—inter–ablation site intervals were obtained from the exported "AblationSites" file. The first annotated application opposite the left inferior PV (tag 24) occurred following completion of tag 23 at the LA appendage ridge, with a prior inter–ablation site interval of 57.3 seconds, indicative of catheter manipulation to and stabilization at the LAPW (Figure 2). Tag 25 commenced 21.9 seconds after tag 24 completion and was annotated at 4.8 mm distance (Figure 3). However, tag 26 commenced 4.7 seconds after tag 25 completion and was annotated at 4.9 mm distance (Figure 4) and tag 27 commenced 3.7 seconds after tag 26 completion, at 5.1 mm distance (Figure 5). Later consecutive tags in this region were annotated at the minimum VISITAG timing intervals, with annotated RF data indicating completion of a 7.3-second application (tag 43, Figure 6), followed by a 36.4-second application commencing 17 ms later at 5.5 mm distance (tag 44, Figure 7), and an 8.3-second application commencing 16 ms later at 6.5 mm distance (tag 45, Figure 8). These last events were likely due to inadvertent catheter displacement, since the minimum RF power for tags 44 and 45 was 29 W. All 11 annotated RF tags in the region of the AEF were delivered during constant catheter-tissue contact: median (range) minimum CF 6 g (1–27 g) (see Figures 9–12 for the remaining LAPW tags).

Discussion

We have provided a detailed description of auto-annotated RF tags from a case of AEF following ablation index–guided

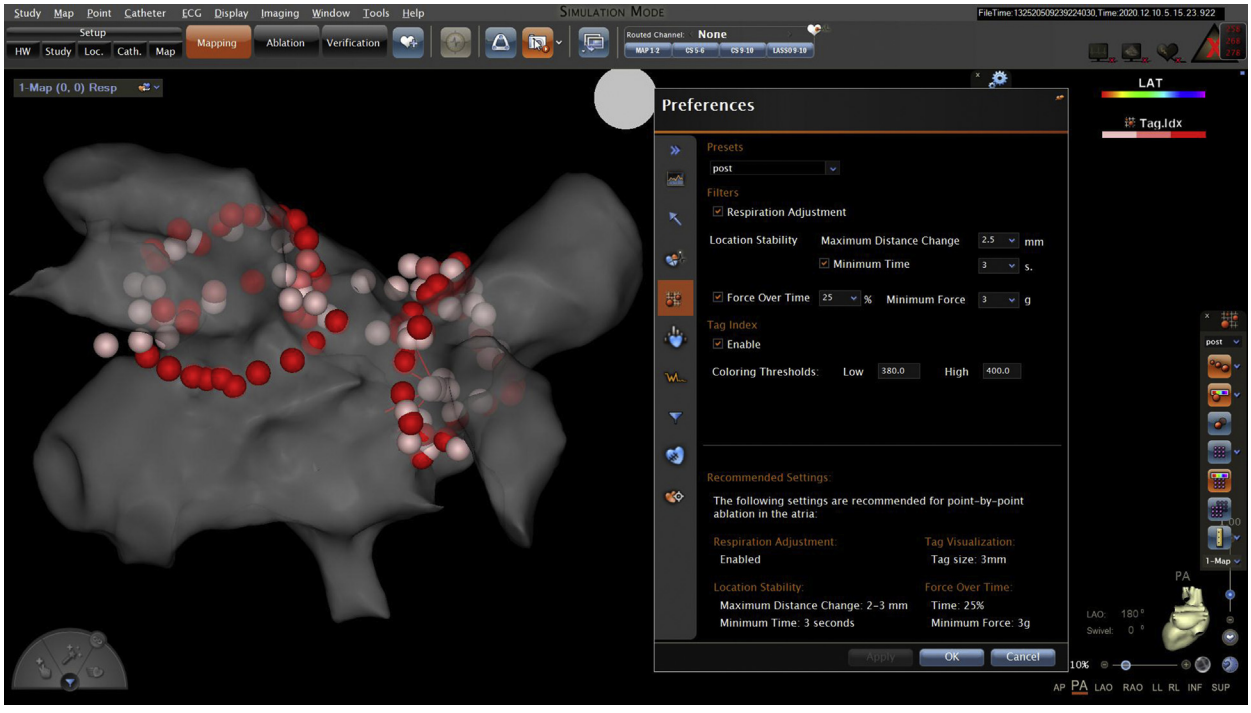

Figure 1 Sites of auto-annotated radiofrequency ablation with tag coloration using ablation index. CARTO (Biosense Webster Inc., Irvine, CA) posteroanterior view with procedural ablation index tag coloration 380–400. VISITAG preferences are shown (*box*); 2 mm tag radius in this image, for clarity.

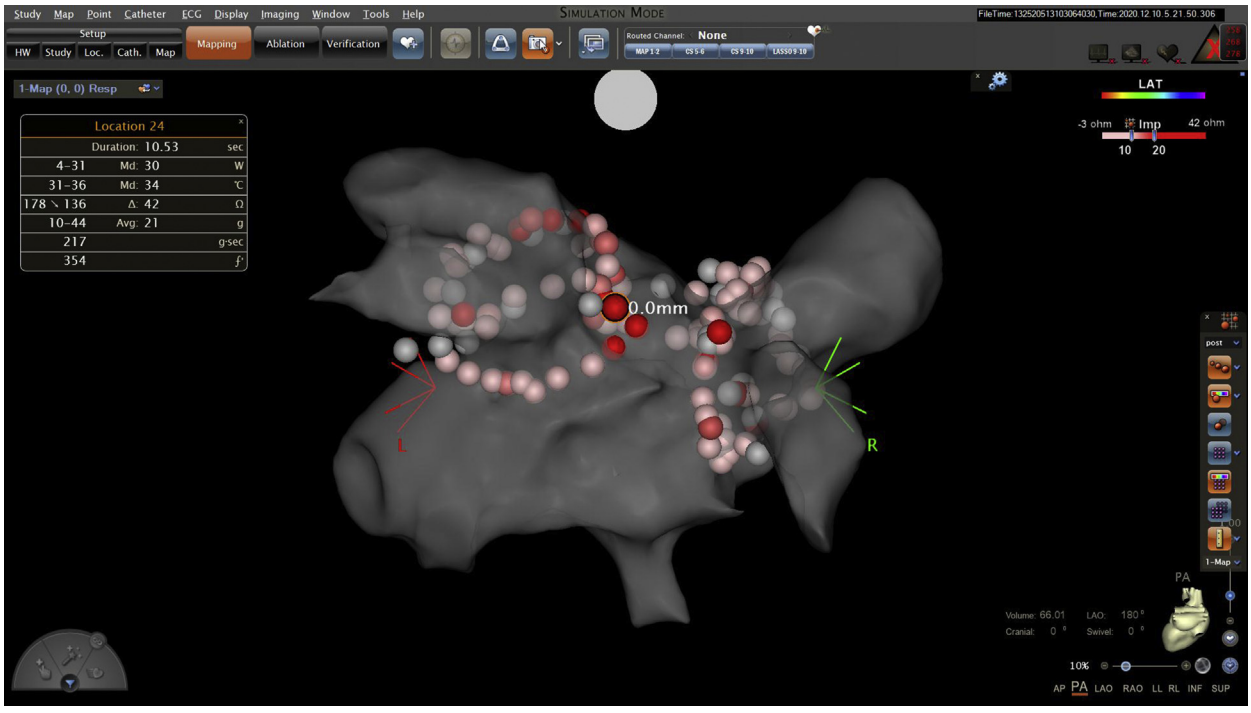

Figure 2 Sites of auto-annotated radiofrequency (RF) ablation with impedance drop coloration. The first lesion in the posterior wall adjacent to the left inferior pulmonary vein (tag 24) is highlighted, showing RF data (*box*, from top to bottom: RF duration; power; tip temperature; impedance (range and drop); contact force (mean and range), force time integral; ablation index).

PVI at 30 W, in the hope that lessons can be learned toward eliminating this tragic complication.

The approach to PVI described here was in keeping with current publications and practice, since CLOSE PVI protocol–derived methods were employed—that is, ablation index ≥400 at the posterior wall, targeting interlesion distance ≤6 mm, using 30 W.[1] However, offline analyses of VISITAG module auto-annotated data demonstrated 3 adjacent LAPW sites constituting the greatest RF-induced tissue effects of the procedure over a small area near the left inferior PV, in the region where AEF later developed. Specifically: (1) the first RF application here demonstrated the greatest impedance drop of the case (42 Ω), resulting from 10.5 seconds RF, AI 354; (2) at the following 2 auto-annotated ablation sites, 21.0 seconds and 19.4 seconds RF were delivered, achieving impedance drop and AI of 23.3 Ω and 418, and 27.2 Ω and 535, respectively; (3) successive sites were each within 6 mm of each other; (4) RF onset at the third site (tag 26) occurred 4.7 seconds after completion of tag 25, raising the possibility of extracardiac thermal trauma owing to "thermal stacking."

Although it is not possible to implicate individual annotated lesions to AEF pathogenesis, this first cluster of applications demonstrating significant RF effect was followed by further RF delivery in this region at a later stage, with this same pattern of (1) significant RF effect, evidenced by high impedance drop over short RF duration, yet with low AI—19.2 Ω impedance drop following 7.3 seconds RF, AI

Table 2 Auto-annotated radiofrequency ablation data at the site of the atrioesophageal fistula

Tag	Intertag time (s)	Distance from prior tag (mm)	Minimum power (W)	Minimum CF (g)	Mean CF (g)	RF duration (s)	Ablation index	Impedance drop (Ω)
24	57.3	NA	4	10	20.6	10.5	354	42.2
25	21.9	4.8	4	6	37.7	21.0	535	23.3
26	4.7	4.9	5	6	16.7	19.4	418	27.2
27	3.7	5.1	5	1	15.2	18.7	406	6.4
43	1.1	5.3	5	8	24.8	7.3	322	19.6
44	0.017	5.5	29	6	16.1	36.4	523	5.4
45	0.016	6.5	29	4	19.6	8.3	329	11.0
46	5.4	3.3	5	3	22.3	38.5	578	9.7
47	24.5	2.2	5	16	33.3	23.7	539	16.1
114	331.0	6.2	5	15	22.9	11.0	378	6.6
115	0.016	5.1	30	27	34.6	3.8	285	NA

CF = contact force; RF = radiofrequency.

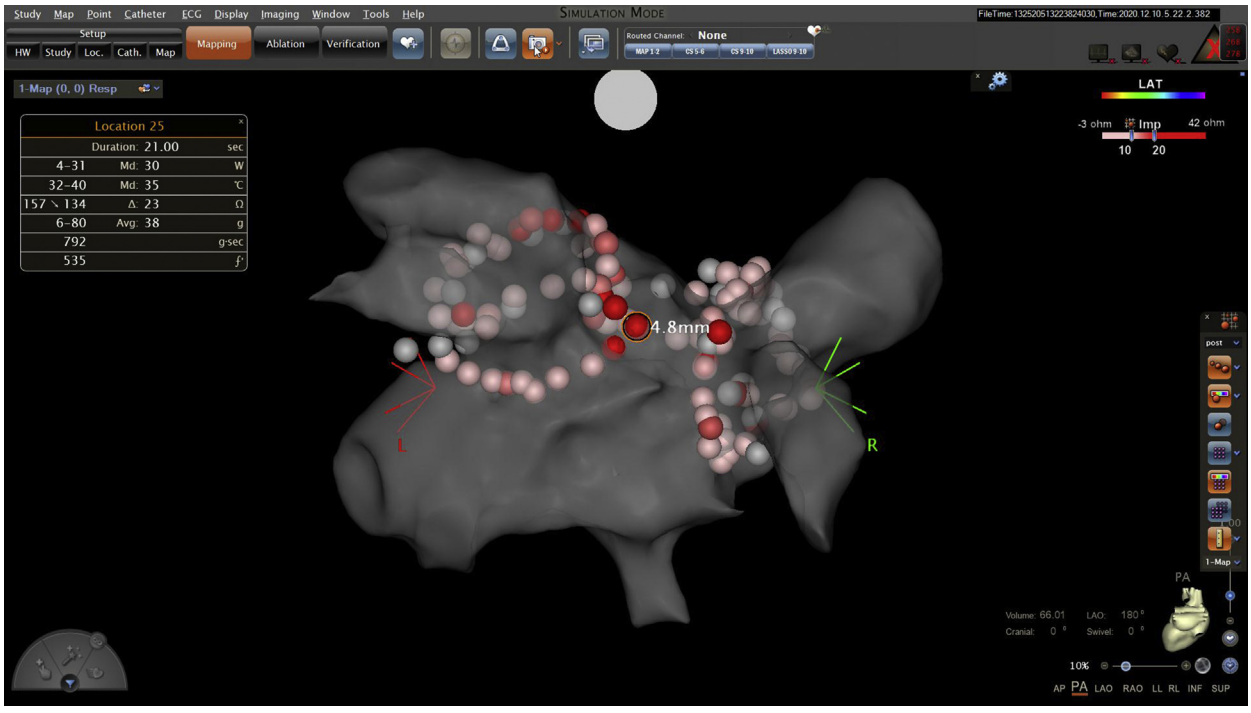

Figure 3 Auto-annotated radiofrequency (RF) tag 25 is highlighted, with accompanying RF data (*box*). RF at this site begins 21.9 seconds following RF completion at tag 24, at a 4.8 mm distance.

322; and (2) consecutive RF applications delivered within 6 mm yet with short inter–ablation site times of 1.1 seconds, 16/17 ms, and 5.4 seconds.

AEF represents an important limitation of any thermal approach toward achieving permanent and transmural ablation effect and is a particularly worrying complication given its high fatality rate.[2] At present, there is no proven means to prevent AEF. Recent reports indicate greater risk of AEF in association with CF RF use,[3,4] with a rate of ~1% in the CIRCA DOSE[5] and AMICA[6] randomized

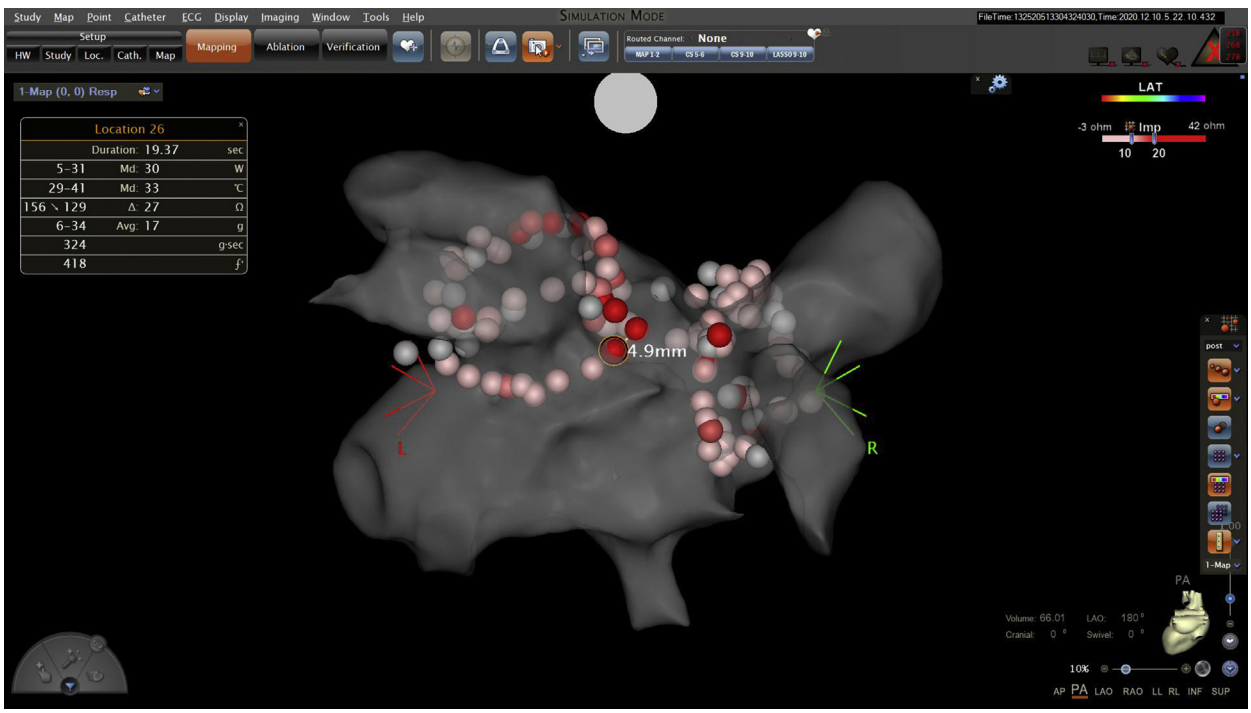

Figure 4 Auto-annotated radiofrequency (RF) tag 26 is highlighted, with accompanying RF data (*box*). RF at this site begins 4.7 seconds following RF completion at tag 25, at 4.9 mm distance.

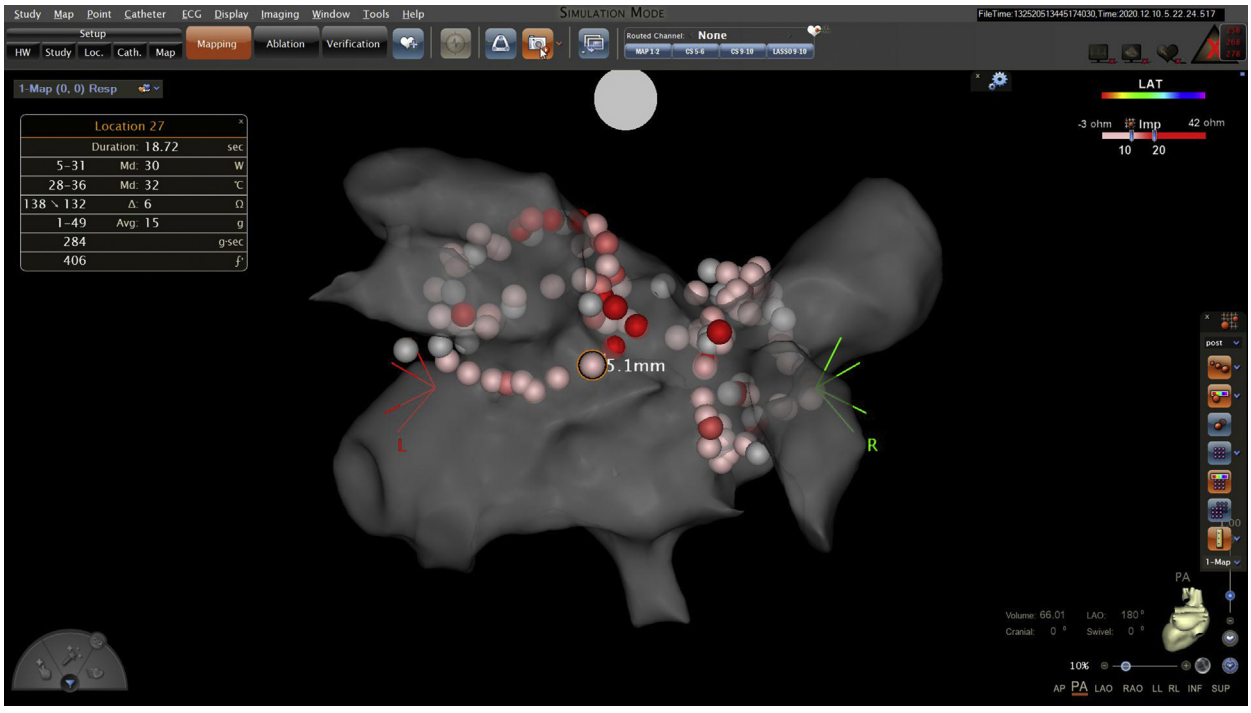

Figure 5 Auto-annotated radiofrequency (RF) tag 27 is highlighted, with accompanying RF data (*box*). RF at this site begins 3.7 seconds following RF completion at tag 26, at 5.1 mm distance.

clinical trials, but recent French national data reported a rate of 0.026%.[7] Esophageal temperature probe monitoring was not used in this present case, but the evidence is inconclusive on whether this would have mattered. Retrospective data demonstrate either significantly increased[8] or decreased[9] occurrence of endoscopically detected esophageal lesions (EDEL) postablation. Esophageal temperature probe use to guide energy delivery was considered "reasonable" (class IIa, level of evidence C) according to the 2017 HRS/EHRA/ECAS/APHRS/SOLAECE expert consensus

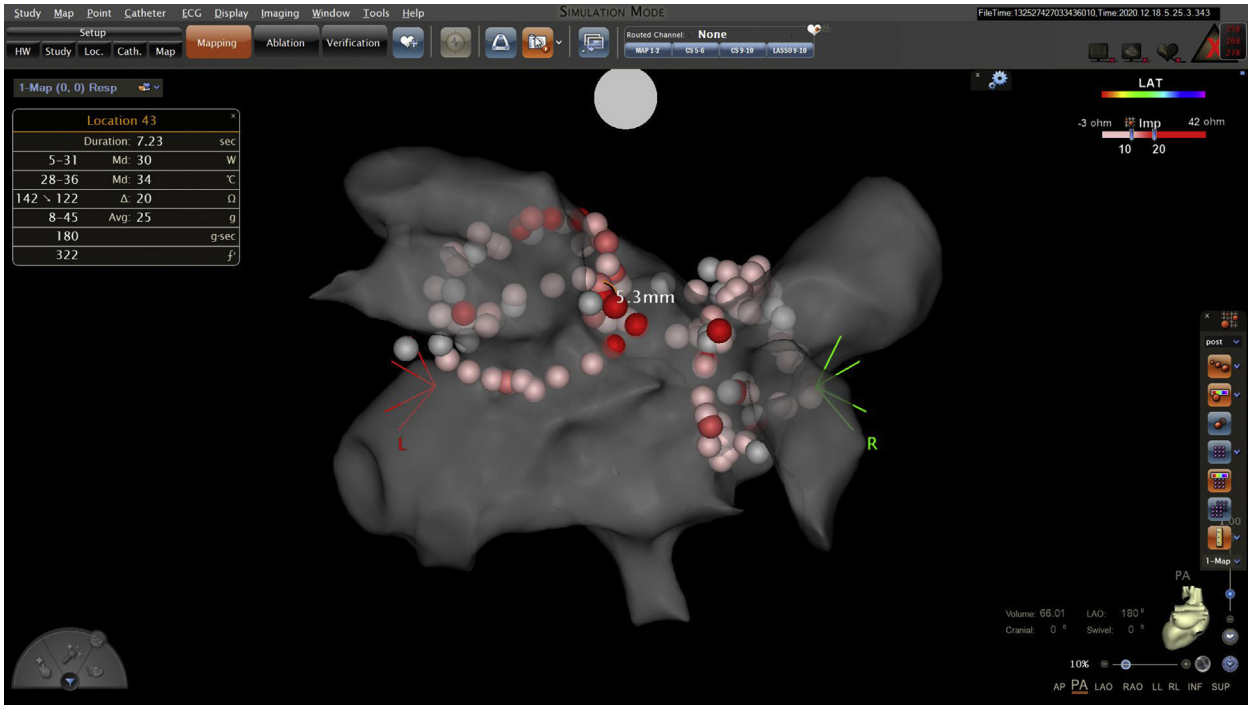

Figure 6 Auto-annotated radiofrequency (RF) tag 43 is highlighted, with accompanying RF data (*box*). At 19.6 Ω this is the fourth-greatest impedance drop site achieved at the left-sided left atrial posterior wall. RF at this site begins 1.1 seconds following RF completion at tag 42, at 5.3 mm distance.

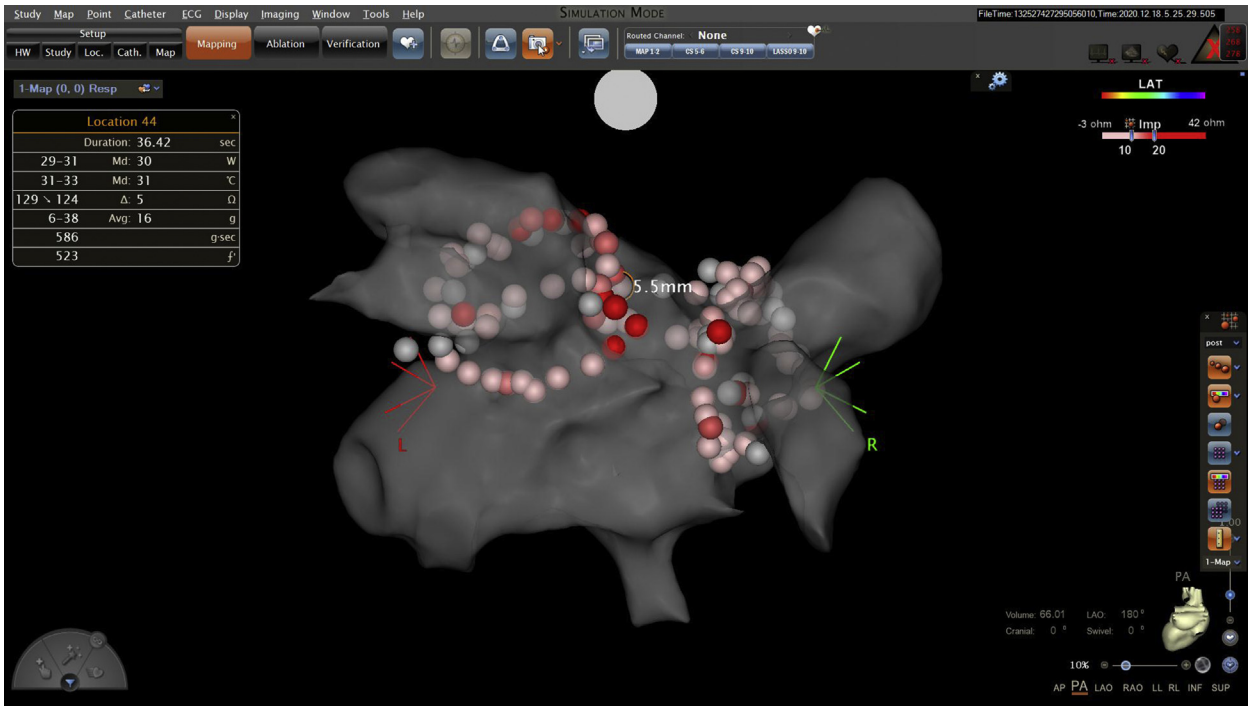

Figure 7 Auto-annotated radiofrequency (RF) tag 44 is highlighted, with accompanying RF data (*box*). RF at this site begins 0.017 seconds following RF completion at tag 43, at 5.5 mm distance. A duration of 36.4 seconds is within guideline recommendations but, when delivered immediately consecutively to another lesion within 6 mm, might create excessive focal RF effect.

statement on catheter and surgical ablation of AF.[10] Yet the recently performed OPERA randomized controlled trial (RCT) demonstrated that SensiTherm esophageal probe temperature monitoring (target <40°C, CF RF at 25–30 W) was without beneficial effect.[11]

A promising technology toward reducing EDEL was demonstrated in IMPACT[12]—an RCT of the ensoETM (Attune Medical, Chicago, IL) esophageal protection device, vs single-sensor temperature probe (Level 1 Oesophageal Temperature Probe; Smiths Medical, Minneapolis, MN: target

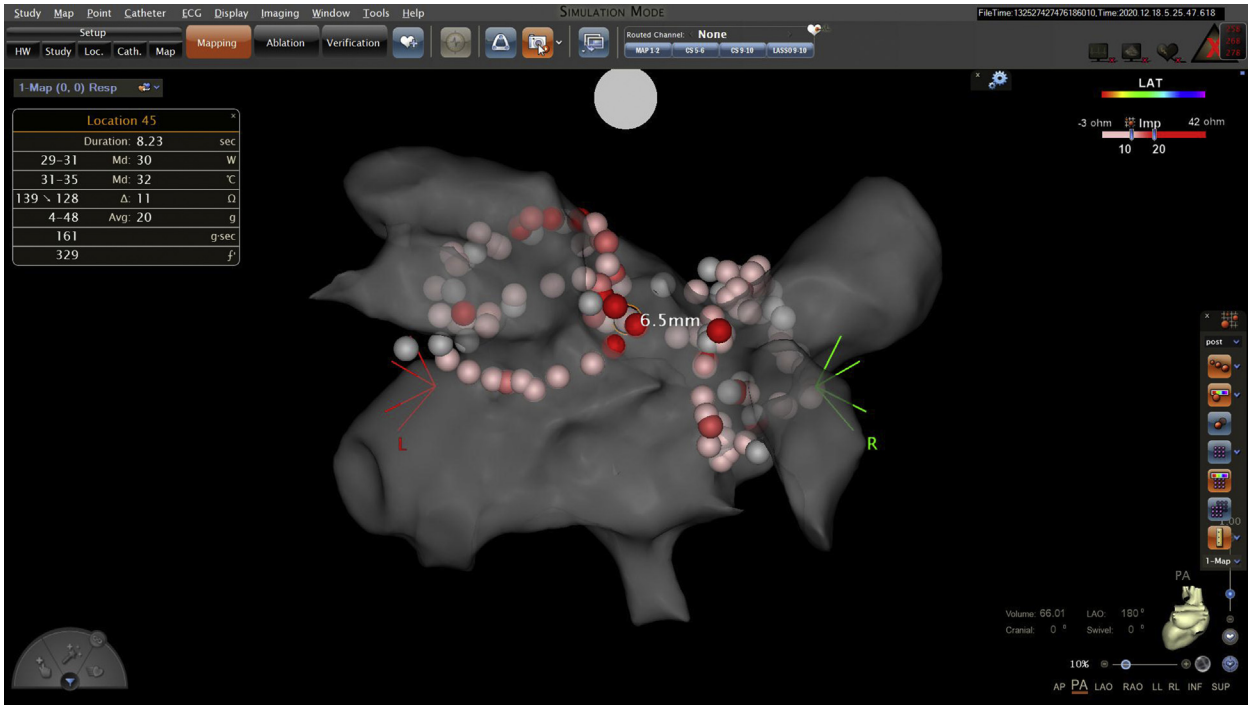

Figure 8 Auto-annotated radiofrequency (RF) tag 45 is highlighted, with accompanying RF data (*box*). RF at this site begins 0.016 seconds following RF completion at tag 44, at a 6.5 mm distance.

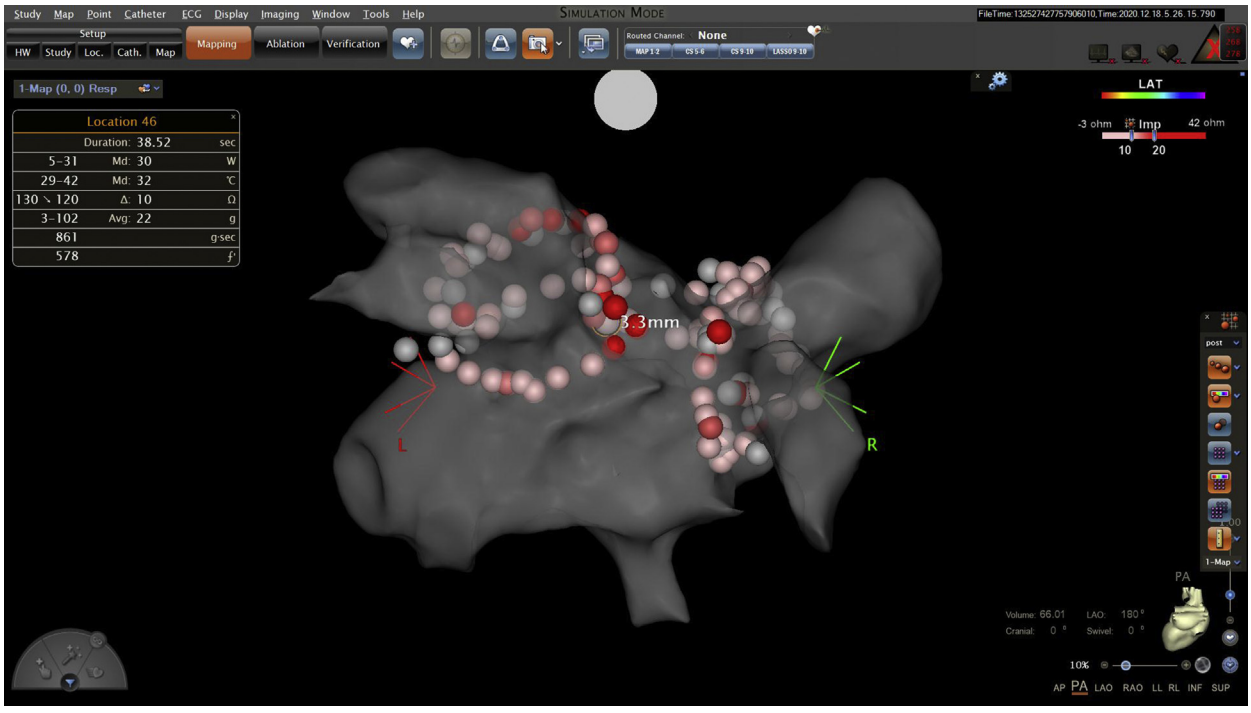

Figure 9 Auto-annotated radiofrequency (RF) tag 46 is highlighted, with accompanying RF data (*box*). RF at this site begins 5.4 seconds following RF completion at tag 45, at 3.3 mm distance. A duration of 38.5 seconds is within guideline recommendations but, when delivered shortly after another lesion within 6 mm, might create excessive focal RF effect. This site is also very close to the previous high impedance drop auto-annotated tags.

$\leq 38^{\circ}$C) during LAPW RF delivery. Using 30 W and with esophageal cooling at 4°C starting at least 10 minutes prior to LAPW RF (posterior wall AI target 350–400), EDEL occurred in 12 of 60 patients without and 2 of 60 with esophageal cooling ($P = .008$). Esophageal cooling will clearly require general anesthesia. Intraprocedural mechanical esophageal deviation has been reported[13] but is yet to undergo RCT. Intraprocedural esophageal imaging with

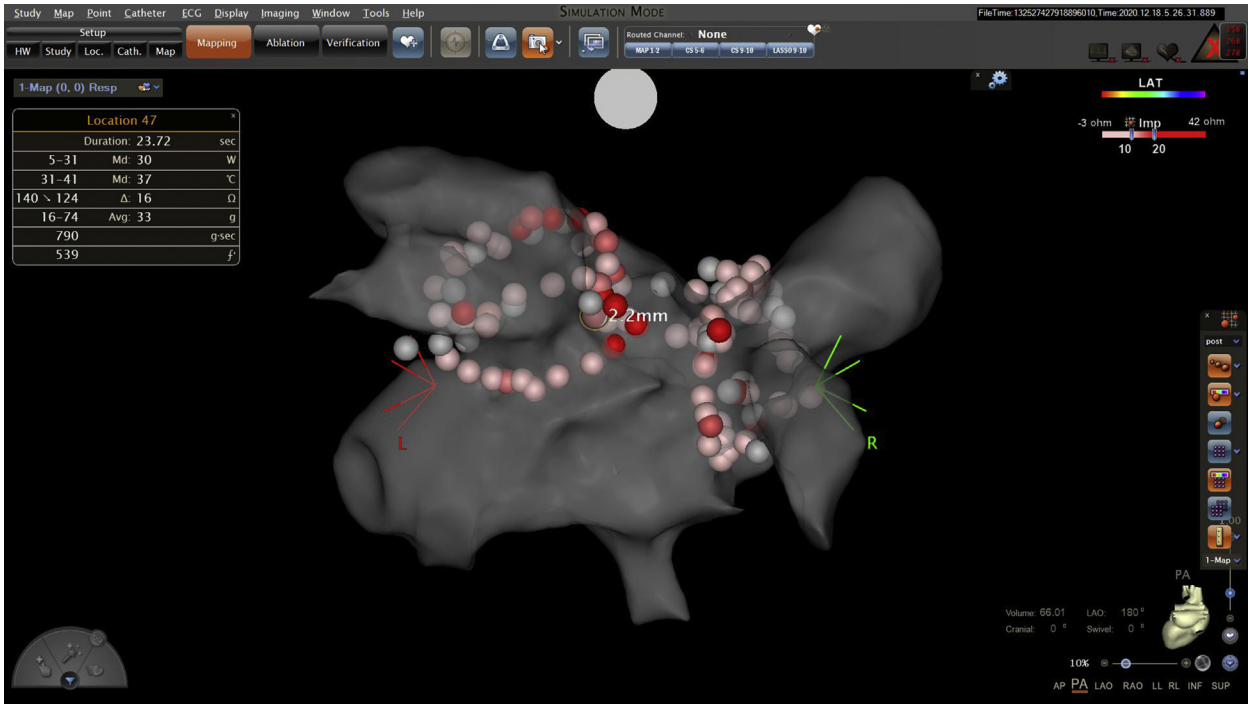

Figure 10 Auto-annotated radiofrequency (RF) tag 47 is highlighted, with accompanying RF data (*box*). RF at this site begins 24.5 seconds following RF completion at tag 46, at 2.2 mm distance. Although 23.7 seconds duration is within guideline recommendations, an impedance drop of 16 Ω might have contributed to excessive focal RF effect and atrioesophageal fistula.

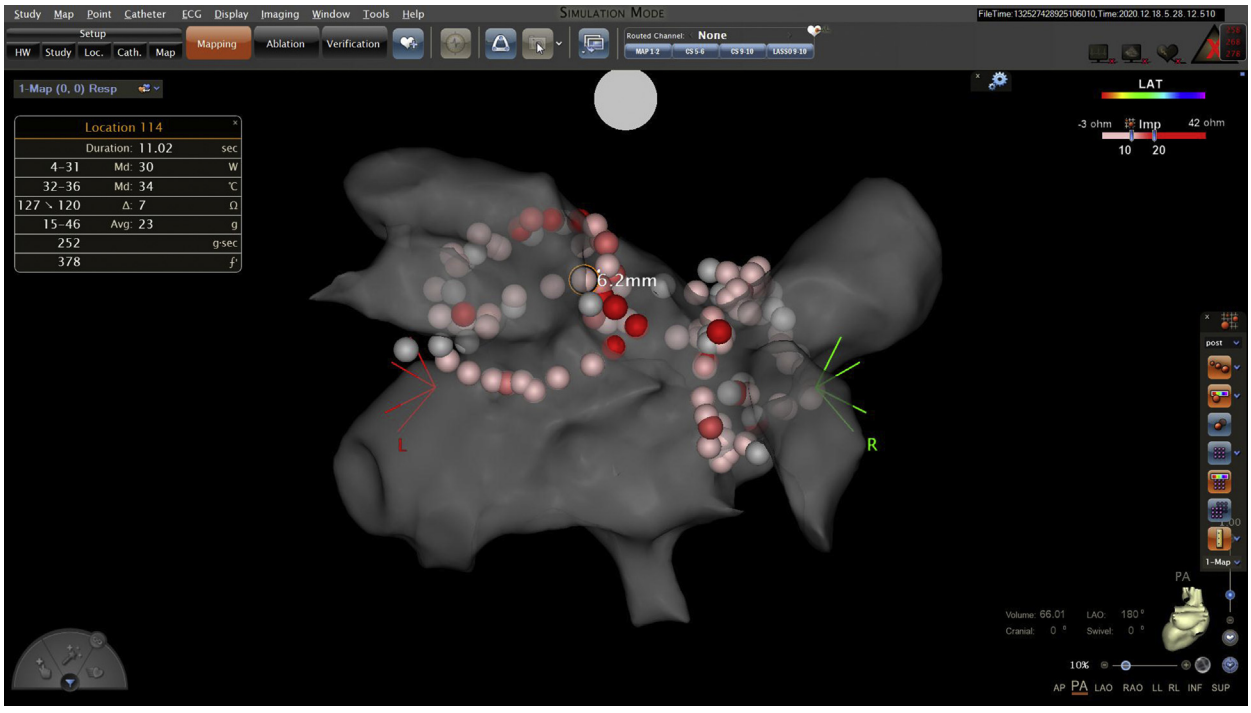

Figure 11 Auto-annotated radiofrequency (RF) tag 114 is highlighted, with accompanying RF data (*box*). RF duration at this site is short and begins 331.0 seconds following RF completion at tag 113, at 6.2 mm distance.

intracardiac echo may also help reduce EDEL, but studies have yet to be performed.

We believe this case report illustrates concepts underlying the in vivo effects of RF energy delivery, with important safety and possibly practice-changing implications:

- Multiple independently conducted investigations have demonstrated clinically important site-specific differences in RF effects during PVI, with the consistent finding of significantly greater RF-induced tissue effects at the left vs right side of the LAPW.[14–17] Preliminary data in

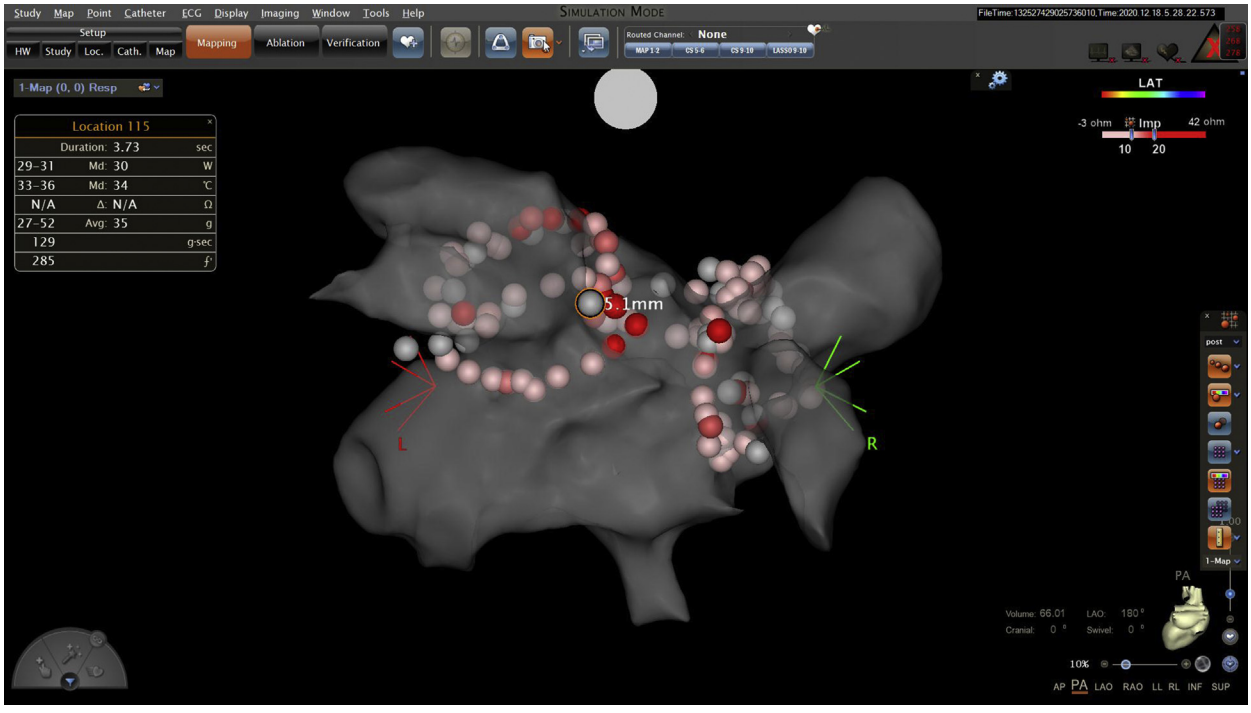

Figure 12 Auto-annotated radiofrequency (RF) tag 115 is highlighted, with accompanying RF data (*box*). RF duration at this site is very short and begins 0.016 seconds following RF completion at tag 114, at 5.1 mm distance.

preprint form suggest that this is driven by a combination of significantly greater surface area of catheter-tissue contact combined with greater in-phase (with tissue motion) catheter stability at left-sided LAPW sites.[18] Unfortunately, the use of AI to guide RF delivery renders an operator blind to site-specific differences in the tissue effects of RF, since neither the surface area of catheter-tissue contact nor out-of-phase catheter-tissue motion (in the setting of stable catheter [x, y, z] position data) are incorporated into AI logic.

- Thermodynamic laws require the possibility of clinically important tissue heating beyond the immediate location of a 3-mm-radius auto-annotated ablation site.[19,20] Therefore, when closely spaced consecutive RF applications occur over short inter–ablation site times, deep RF effects resulting from higher starting tissue temperatures at subsequently targeted sites may be excessive, risking later AEF formation. Presently, auto-annotation-guided protocols for RF delivery fail to account for this factor.

Furthermore, "lesion indexing" (eg, AI / lesion size index) was developed using small patient numbers and was intended to primarily inform procedural efficacy and efficiency rather than safety. Systematic studies of EDEL following ablation index–guided RF delivery demonstrate mild vs severe esophageal lesions in 14% vs 3% of patients, respectively, even when targeting AI $\leq$350.[21]

Therefore, instead of relying on inaccurate surrogate markers of RF delivery, such as AI or lesion size index (LSI; Abbott Inc., IL), methods with theoretically greater validity toward assessing the tissue response to heating include an assessment of auto-annotated impedance drop[22,23] and the timing of unipolar electrogram morphology change from RS to pure R.[24,25]

Clearly, the precise details of any methodological enhancements toward greater safety require investigation in clinical trials, but, given the strong evidence base underlying the heterogeneity in RF effect at the LAPW, we believe that patients are likely to benefit from the immediate introduction of impedance monitoring and maximum impedance drop safety cut-offs. On this point it is noteworthy that a recent publication describing AI-guided PVI using 50 W incorporated a safety measure of impedance graph visualization, with RF termination in the event of "per-site" impedance drop >40 Ω.[26] Furthermore, Boston Scientific Inc has developed an impedance-based system—local impedance—for lesion assessment as the foundation of its RF ablation platform.

Conclusion

This report of AI-guided PVI at 30 W, which resulted in AEF, demonstrates important auto-annotated RF findings. Specifically, closely spaced RF applications were delivered at the left side of the LAPW over short inter–ablation site time intervals and at each site there were high levels of tissue heating, evidenced by greatest annotated impedance drops of the entire procedure. Together, these findings indicate that AI guidance alone represents an imperfect means to perform PVI with optimal safety. Furthermore, that the RF power, target inter–ablation site distance, and AI targets employed were within current practice criteria indicates the important flaws of any RF delivery protocol failing to account for thermodynamic laws and the proven significantly greater RF effects at left- vs right-sided LAPW sites. It is our hope that once recognized, such knowledge will be incorporated into novel clinical protocols, thereby improving the safety of AF ablation without compromising efficacy.

Acknowledgments

We are grateful for the patient's family giving us their permission to submit this case report, toward helping the electrophysiology community better understand how to avoid atrioesophageal fistula.

References

1. Phlips T, Taghji P, El Haddad M, et al. Improving procedural and one-year outcome after contact force-guided pulmonary vein isolation: the role of interlesion distance, ablation index, and contact force variability in the 'CLOSE'-protocol. Europace 2018;20:f419–f427.
2. Mohanty S, Santangeli P, Mohanty P, et al. Outcomes of atrioesophageal fistula following catheter ablation of atrial fibrillation treated with surgical repair versus esophageal stenting. J Cardiovasc Electrophysiol 2014; 25:579–584.
3. Black-Maier E, Pokorney SD, Barnett AS, et al. Risk of atrioesophageal fistula formation with contact force–sensing catheters. Heart Rhythm 2017; 14:1328–1333.
4. Medeiros De Vasconcelos JT, Filho S dos SG, Atié J, et al. Atrial-oesophageal fistula following percutaneous radiofrequency catheter ablation of atrial fibrillation: the risk still persists. Europace 2016;19:euw284.
5. Andrade JG, Champagne J, Dubuc M, et al. Cryoballoon or radiofrequency ablation for atrial fibrillation assessed by continuous monitoring: a randomized clinical trial. Circulation 2019;140:1779–1788.
6. Kuck K-H, Merkely B, Zahn R, et al. Catheter ablation versus best medical therapy in patients with persistent atrial fibrillation and congestive heart failure: the randomized AMICA trial. Circ Arrhythm Electrophysiol 2019;12:e007731.
7. Gandjbakhch E, Mandel F, Dagher Y, Hidden-Lucet F, Rollin A, Maury P. Incidence, epidemiology, diagnosis and prognosis of atrio-oesophageal fistula following percutaneous catheter ablation: a French nationwide survey. Europace 2021;23:557–564.
8. Müller P, Dietrich J-W, Halbfass P, et al. Higher incidence of esophageal lesions after ablation of atrial fibrillation related to the use of esophageal temperature probes. Heart Rhythm 2015;12:1464–1469.
9. Kiuchi K, Okajima K, Shimane A, et al. Impact of esophageal temperature monitoring guided atrial fibrillation ablation on preventing asymptomatic excessive transmural injury. J Arrhythmia 2016;32:36–41.
10. Calkins H, Hindricks G, Cappato R, et al. 2017 HRS/EHRA/ECAS/APHRS/SOLAECE expert consensus statement on catheter and surgical ablation of atrial fibrillation. Heart Rhythm 2017;14:e275–e444.
11. Schoene K, Arya A, Grashoff F, et al. Oesophageal Probe Evaluation in Radiofrequency Ablation of Atrial Fibrillation (OPERA): results from a prospective randomized trial. Europace 2020;22:1487–1494.
12. Leung LWM, Bajpai A, Zuberi Z, et al. Randomized comparison of oesophageal protection with a temperature control device: results of the IMPACT study. Europace 2021;23:205–215.
13. Bhardwaj R, Naniwadekar A, Whang W, et al. Esophageal deviation during atrial fibrillation ablation: clinical experience with a dedicated esophageal balloon retractor. JACC Clin Electrophysiol 2018;4:1020–1030.
14. Knecht S, Reichlin T, Pavlovic N, et al. Contact force and impedance decrease during ablation depends on catheter location and orientation: insights from pulmonary vein isolation using a contact force-sensing catheter. J Interv Card Electrophysiol 2015;43:297–306.
15. Chelu MG, Morris AK, Kholmovski EG, et al. Durable lesion formation while avoiding esophageal injury during ablation of atrial fibrillation: lessons learned

from late gadolinium MR imaging. J Cardiovasc Electrophysiol 2018; 29:385–392.
16. Tomlinson DR, Myles M, Stevens KN, Streeter AJ. Transmural unipolar electrogram change occurs within 7 s at the left atrial posterior wall during pulmonary vein isolation. Pacing Clin Electrophysiol 2019;42:922–929.
17. Das M, Luik A, Shepherd E, et al. Local catheter impedance drop during pulmonary vein isolation predicts acute conduction block in patients with paroxysmal atrial fibrillation: initial results of the LOCALIZE clinical trial. EP Europace 2021;23:1042–1051.
18. Tomlinson DR. Mechanistic insights into heterogeneous radiofrequency ablation effects at the left atrial posterior wall during pulmonary vein isolation [abstract]. medRxiv 2019;19008706. https://doi.org/10.1101/19008706.
19. Tomlinson DR, Stevens KN, Streeter AJ. Assessment of the transmural unipolar electrogram morphology change radius during contact force-guided pulmonary vein isolation using the VISITAG^{TM} Module and CARTOREPLAY^{TM}. bioRxiv 2018;284539. https://doi.org/10.1101/284539.
20. Barbhaiya CR, Kogan EV, Jankelson L, et al. Esophageal temperature dynamics during high-power short-duration posterior wall ablation. Heart Rhythm 2020; 17:721–727.
21. Halbfass P, Berkovitz A, Pavlov B, et al. Incidence of acute thermal esophageal injury after atrial fibrillation ablation guided by prespecified ablation index. J Cardiovasc Electrophysiol 2019;30:2256–2261.
22. Avitall B, Mughal K, Hare J, Helms R, Krum D. The effects of electrode-tissue contact on radiofrequency lesion generation. Pacing Clin Electrophysiol 1997; 20:2899–2910.
23. Nsah E, Berger R, Rosenthal L, et al. Relation between impedance and electrode temperature during radiofrequency catheter ablation of accessory pathways and atrioventricular nodal reentrant tachycardia. Am Heart J 1998; 136:844–851.
24. Pambrun T, Roig J, Bouzeman A, et al. Modification of the unipolar atrial electrogram as a local endpoint during common atrial flutter ablation. J Cardiovasc Electrophysiol 2015;26:1196–1203.
25. Pambrun T, Durand C, Constantin M, et al. High-power (40–50 W) radiofrequency ablation guided by unipolar signal modification for pulmonary vein isolation. Circ Arrhythm Electrophysiol 2019;12:e007304.
26. O'Brien J, Obeidat M, Kozhuharov N, et al. Procedural efficiencies, lesion metrics, and 12-month clinical outcomes for Ablation Index-guided 50Wablation for atrial fibrillation. Europace 2021;23:878–886.